Inorganic Chemistry

Article

pubs.acs.org/IC

pH-Responsive Dual Cargo Delivery from Mesoporous Silica Nanoparticles with a Metal-Latched Nanogate

Derrick Tarn, Min Xue, and Jeffrey I. Zink*

Department of Chemistry and Biochemistry, California NanoSystems Institute, University of California, Los Angeles, California 90095, United States

Supporting Information

ABSTRACT: A nanogate composed of two iminodiacetic acid (IDA) molecules and a metal ion latch was designed, synthesized, and assembled on mesoporous silica nanoparticles. This gating mechanism is capable of storing and releasing metal ions and molecules trapped in the pores. Pore openings derivatized with IDA can be latched shut by forming a bis-IDA chelate complex with a metal ion. This system was tested by loading with Hoechst 33342 as the probe cargo molecule, and latching with cobalt, nickel, or calcium metal ions. No cargo release was observed in a neutral aqueous environment, but both cargoes were delivered after acid stimulation and/or the addition of a competitively binding ligand.

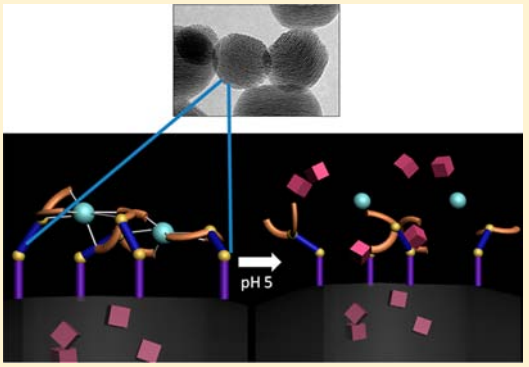

INTRODUCTION

Nanoparticles of MCM-41 silica, a type of mesoporous nanomaterial, have found a variety of applications in many fields.[1−6] In the area of drug delivery, their large pore volume, easily accessible pores, well-established surface chemistry, and high rate of endocytosis by mammalian cells make them versatile nanocontainers.[4,5,7−10] Nanomachines are increasingly being employed on mesoporous silica nanoparticles (MSNs) for stimuli-responsive delivery of cargo molecules from the pores. Numerous organo-functionalized silicas have been designed on MSNs for the purpose of pore control. Researchers have exploited a creative variety of both covalent and noncovalent systems to achieve this goal, including supramolecular nanovalves,[11−17] snap-tops,[18] polymer networks,[19] metal nanocrystals,[20] biomolecules,[21] light-responsive nanogates,[22] magnetic-field-responsive nanogates,[23] nanoimpellers,[24] cleavable chemical bonds,[25] and hydrophobicity.[26] These methods have demonstrated the stimulated release of a variety of ∼1−2 nm sized cargo molecules, but are unable to hold back small metal ions in pores. Reversible chelation on nanoparticles has been used to bind and release metal ions, but did not trap and release molecules from pores.[27−29]

Many metal ions play important biological roles and are the active center of enzymes, proteins, vitamins, and coenzymes.[30,31] Calcium is heavily regulated in eukaryotic cells as a reflection of its important role in a number of physiological processes, notably in orchestrating apoptosis.[32,33] Normally regulated and stored in the endoplasmic reticulum and mitochondria inside cells, calcium stimulates an apoptotic cycle when present in the cell cytoplasm.[34,35] MSNs have been shown to be endocytosed by cells, resulting in colocalization in endosomes and finally endosomal escape through a "proton sponge effect" that results in payload delivery to the cell cytoplasm. Endosomal pH can be as low as 4.5 and more commonly in the range of pH 5−7.[17] Delivery of traditional anticancer drugs with MSNs has also shown high efficacy and cell killing compared to the free drug.[17] A system capable of delivering both therapeutic cargo molecules and biorelevant metal ions would be more efficient than single cargo nanocarriers and could take advantage of synergistic interactions. In this paper, we demonstrate a method that utilizes coordination chemistry in order to achieve the objective of carrying and releasing both metal ions and biologically useful organic cargo molecules from MSNs.

RESULTS AND DISCUSSION

Design of the Gate. In the design of this system, a swinging gate with a latch was synthesized and assembled on MSNs to control pore access. Two gates freely swinging on hinges can be locked in place with a latch. The latch serves a dual purpose of being a desired cargo type and latching the gates shut. When situated around the pore openings, these gates regulate the entrance to the pore interiors (Figure 1b). Cargo molecules are free to diffuse in and out of the pores when the gates are unlatched, but when a metal ion is present, cargo is trapped as a result of latching the nanogate shut. Using this design strategy, iminodiacetic acid (IDA), a chelating agent, is selected as the gate and a metal ion integrated as the latch.

Iminodiacetic acid has a chelating property similar to that of one-half of an ethylenediaminetetraacetic acid (EDTA) molecule. When IDA is attached to silica with a flexible linker,

Received: November 6, 2012
Published: February 7, 2013

   dx.doi.org/10.1021/ic3024265 | Inorg. Chem. 2013, 52, 2044−2049

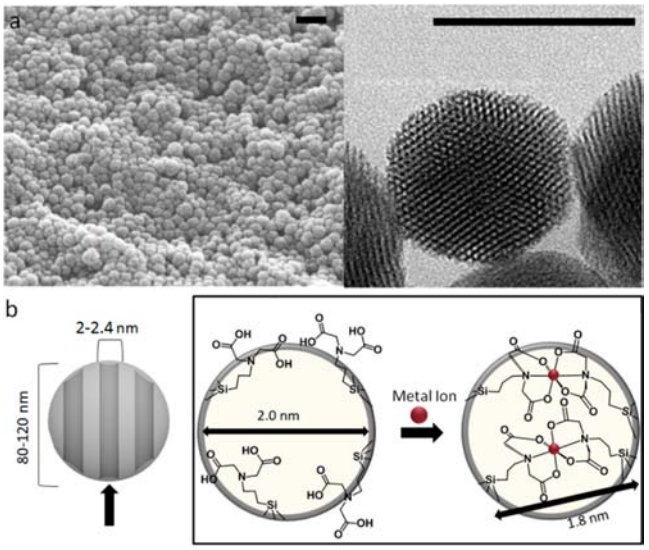

Figure 1. (a) SEM (left) and TEM (right) images of typical batches of MSN. The scale bar for SEM is 200 nm, and that for TEM is 100 nm. The TEM image shows the hexagonally arranged pore channels. (b) Projection down the pore channels of MSN grafted with IDA. In the open state, the single tethered IDA is freely swinging and allows access to the pore channels, but the addition of a metal ion creates an inorganic complex tethered at two ends over the pore opening.

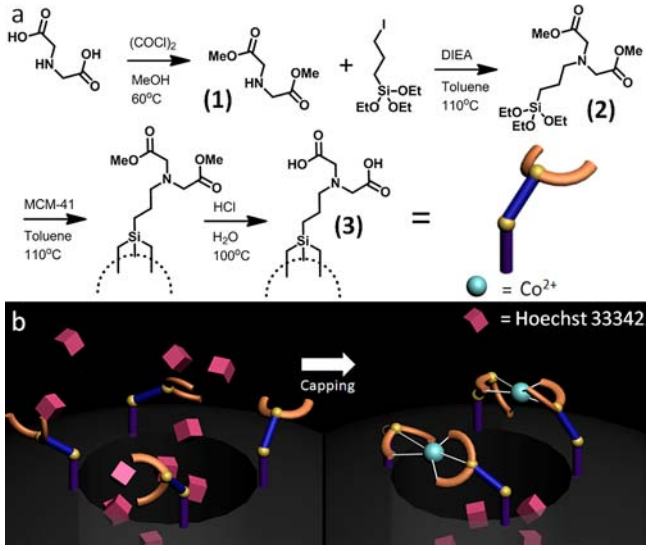

Figure 2. (a) Reaction scheme showing the synthesis and attachment of IDA to the nanoparticle surface. (b) Illustration of the machine assembly process. IDA-modified MCM-41 nanoparticles were loaded with Hoechst 33342, and the nanogate was latched through the introduction of $CoCl_2$. The assembled nanogate was washed to remove surface-adsorbed dye and unbound cobalt.

two neighboring IDA molecules can bind strongly to a metal ion. The IDA binding constant with various metal centers exhibits an $\sim 10^3$ decrease upon changing the pH from neutral to mildly acidic as a result of protonation of the Lewis base chelating groups.[28,29] This property is the basis for the mechanism of operation of the pH-responsive nanogate. A flexible linker bonded to the amine moiety results in one point of attachment to the nanoparticle surface, creating a potentially tridentate ligand that is free to swing when unlatched. The introduction of a metal ion results in a bis-IDA complex, joining two IDA molecules to the metal ion, forming $M(IDA)_2$ tethered to the MSN at the end of each ligand. When the chelation occurs over a pore opening, the system can trap and release molecules into and from the pores (Figure 1b). Since IDA can form stable complexes with many different transition-metal ions,[36,37] this system can function with a variety of different metal latches. Co^{2+}, Ni^{2+}, and Ca^{2+} (that have 10^7, 10^8, and 10^2 order of magnitude formation constants, respectively) were chosen for this study.[37,38]

MSNs were synthesized using a surfactant-templated sol−gel process producing spherical nanoparticles ~100 nm in diameter. Acid removal of the templating agent resulted in hexagonally arranged mesopores about 2.2 nm in diameter (Figure 1a; Supporting Information). Because of the aqueous synthesis conditions, MSNs have a high surface silanol density and additional treatments to functionalize the particles are not required. The IDA swinging gates were attached to the silanols through a postsynthesis grafting method shown in Figure 2.[39]

Because of its existence as a zwitterion, IDA required conversion to an ester in order to allow for nucleophilic substitution to the halogenated alkoxysilane. This was accomplished by reacting IDA with oxalyl chloride in methanol, and nucleophilic substitution of 3-iodopropyltriethoxysilane. The triethoxysilane intermediate was attached to the particle surface through a condensation reaction with surface Si-OH (see the Experimental Section). After grafting on the particle surface, the methyl ester was hydrolyzed to restore IDA (Figure 2a).

Characterization. Synthesized MSN quality was confirmed through XRD and TEM measurements. TEM was used to confirm the distribution of particle sizes between 80 and 120 nm. Image analysis software of nanoparticles viewed directly down the axis of the pore structure showed that the nanoparticles had pore diameters of 2.2 nm (Figure S1, Supporting Information; Figure 1a). The hexagonal pore arrangement observed in Figure 1a is confirmed by higher-order Bragg peaks shown in the powder XRD, which can be indexed as the (100), (110), and (200) planes (Figure S2, Supporting Information) with a lattice spacing of 4 nm. Complete removal of the templating agent was confirmed with FTIR spectroscopy with the disappearance of the C−H stretching peaks at 3000 cm^{-1} after acid extraction (Figure S3, Supporting Information). The synthesis of compounds **1** and **2** was verified with ^1H NMR (see the Experimental Section). Successful attachment of the nanogate was confirmed through CP-MAS solid-state ^{29}Si NMR with the appearance of two signals at −54 and −72 ppm as di- and trifunctionalized Si-C (Figure S4b, Supporting Information), respectively. Additionally, a carbonyl peak was observed in solid-state ^{13}C NMR at 149 ppm, a corresponding α-carbon at 128 ppm, and the aliphatic carbons appearing between 10 and 50 ppm, which indicates a successful attachment of the nanogate thread (Figure S4a, Supporting Information).

Loading and Release. After confirmation of successful attachment of the nanogate, the machine was assembled through a process of loading an organic molecule, latching the gates with a metal ion, and washing away any excess cargo. Hoechst 33342, a dye commonly used as a nuclear stain in cells, was chosen as the probe for its ease of detection and its similar size characteristics to those of therapeutic drugs. By monitoring the fluorescence intensity of Hoechst, a real-time release profile can be generated. From previous studies of grafted molecules, we estimate an average of four gates around each pore opening,

dx.doi.org/10.1021/ic3024265 | Inorg. Chem. 2013, 52, 2044−2049

corresponding to two assembled nanogates per pore (Figure 1b).[15] On the basis of molecular size estimates, when closed, this number of nanogates is more than enough to prevent leakage of cargo molecules between 1 and 2 nm. Loading of Hoechst dye was accomplished by suspending IDA-modified nanoparticles in a concentrated solution of the dye and allowing sufficient time for the dye molecules to diffuse inside the pores.

Cobalt Latch. The Hoechst-loaded nanoparticles were latched shut after introducing a metal ion. Cobalt was chosen as the first metal latch because of its stability, solubility, and large binding constant with IDA. Introducing the Co^{2+} ion latches the nanogates together by bringing two IDA units together (Figure 2b). To remove any surface-adsorbed Hoechst and unbound cobalt, the pale yellow particles were washed with aliquots of fresh ddH_2O until the rinses no longer exhibited any fluorescence.

To assess the functioning of the nanogates, release of Hoechst dye was monitored using a time-resolved fluorescence spectroscopy method. The fully assembled and latched nanoparticles were placed in a corner of a glass cuvette, and an excitation beam (377 nm) was used to excite any dye released into the supernatant (Figure S7, Supporting Information). The corresponding emission spectrum was collected to generate a time-resolved release profile.

Acid Release. After collecting baseline fluorescence, the machine was activated by slightly acidifying the solution. Trace 1 in Figure 3a shows that, at neutral pH, no Hoechst fluorescence is detected, indicating no observable cargo leakage of Hoechst molecules at neutral pH. After adjusting the solution to a pH of 5, a large increase in solution fluorescence is observed, indicating a release of Hoechst molecules from the pores into solution stimulated by the acidification. To differentiate between surface-adsorbed dye from dye stored in the pores and to assess hydrogen-bonding strengths between IDA dimers, a control experiment was performed where IDA-modified particles were loaded with Hoechst, but left unlatched by omitting the cobalt attachment step. This sample was subjected to a similar washing procedure and "released" by adjusting the solution pH to 5. Trace 3 in Figure 3a shows no Hoechst release after acidification, indicating that the loaded Hoechst cargo was removed during the washing steps. This also indicates that the amount of positively charged Hoechst adsorbed on the surface silanols (which ionize into $Si\text{-}O^-$ at neutral pH)[40] is insignificant when compared to the amount capable of being stored and delivered through pore control (Figure 3b). Additionally, hydrogen bonding between two IDA dimers does not result in unintentionally latching the nanogates and holding back cargo.

After completion of each time-resolved fluorescence spectra, the amount of cobalt removed from the nanogates was analyzed through ICP-OES analysis. For the sample loaded with Hoechst and latched with cobalt, the addition of acid resulted in cobalt unbinding (Figure 3b1). Because of the strength of the electrostatic interaction between doubly cationic cobalt and surface $Si\text{-}O^-$ groups, Co^{2+} was difficult to completely remove from the particle surface with washings. As a result, after subjecting Hoechst-loaded cobalt-latched nanoparticles to a 24 h soaking period, a small quantity of cobalt was still removable from the particle surface (Figure 3b2). It is important to note that this unbinding of cobalt is not coupled with Hoechst cargo release. This result indicates that at least two differently bound forms of cobalt are removed from MSN: surface-adsorbed cobalt as a result of electrostatic interactions with silica, and chelated cobalt bound in the IDA nanogates.

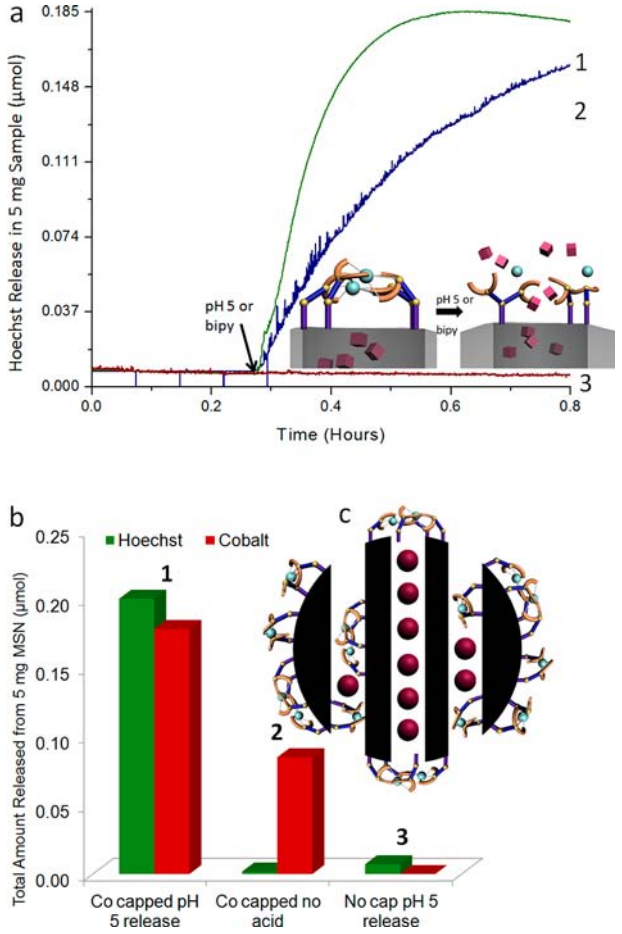

Figure 3. (a) Time-resolved fluorescence spectra showing the release of Hoechst dye from the gated pores. (Trace 1) Cargo is observed to release from the pores upon changing the solution pH to 5. (Trace 2) Release is also observed when 2,2′-bipyridine is added to the solution, since the competing chelator is capable of removing the metal latch from the nanogate. (Trace 3) No release of Hoechst is observed from Hoechst-loaded IDA-modified particles when no metal ion is introduced and the nanogate is left unlatched. (b) 1. The total amount of Hoechst and cobalt (in μmol) released from 5 mg of nanomachine. 0.2 μmol of Hoechst released corresponds to a 2% weight release, and 1.8 μmol of cobalt released corresponds to a 0.2% weight release. 2. Hoechst-loaded, cobalt-latched nanoparticles are subjected to a 24 h soaking period in which a 1% weight release of cobalt is detected, but no Hoechst release. 3. Hoechst-loaded IDA-modified MSNs are "released" by adjusting the solution pH to 5, resulting in a trivial amount of Hoechst released. (c) Cobalt ions are released not only from the latched nanogates but also from ligands attached elsewhere on the particle.

After complete release, the total weight percent of dye was calculated through UV−vis absorption measurements of the solution supernatant. The observed 2% weight of Hoechst is a typical delivery capacity of MSNs loaded with Hoechst.[41] Additionally, a 0.2% weight release of cobalt was observed. In terms of molar concentration, this amount is on the order of Hoechst released; 5 mg of gated particles can release ~0.2 μmol of Hoechst and cobalt, demonstrating that the system is capable of delivering comparable molar quantities of both cargo types (Figure 3b1). The large amount of cobalt released can be explained through examining the pore structure of MCM-41.

dx.doi.org/10.1021/ic3024265 | Inorg. Chem. 2013, 52, 2044−2049

Only nanogates present across the pore openings function in controlling Hoechst delivery. However, some derivatization of the particles with IDA also occurs on the outer surface, resulting in sites for metal ion chelation not used to control pore access but acting as cobalt storage (Figure 3c). Because of the large excess of cobalt used in latching the nanogate, these nongating IDA moieties can also chelate cobalt, resulting in the large amount of cobalt released after acidification.

Competitive Binding Release. Since the nanogate trapping is dependent on the coordination of the metal center, removal of the metal center by a strong chelating agent dissolved in solution should also result in cargo release. To examine this, the cobalt-latched nanogate was exposed to a molecule capable of competitively binding cobalt from IDA. Figure 3a, trace 2, demonstrates that the addition of 2,2′-bipyridine (bipy) to the system results in the release of Hoechst cargo. Therefore, a second release method based on competitive binding is also possible. If a ligand that has a large binding constant with the metal ion is added to the system, that ligand competes with the IDA, binds with the metal, and thus opens the system. This result demonstrates that the removal of the metal center by a competing ligand unlatches the gate, resulting in cargo delivery.

Nickel Latch. Since the amine and carboxylic acid groups on IDA can form strong coordinational bonds with a variety of transition metals, Ni^{2+} was also tested for a viable latch. Studies were performed using the same procedures as previously described. After loading with Hoechst cargo and latching the nanogate by introducing Ni^{2+}, a baseline fluorescence was collected at neutral pH to verify the stability of the assembled machine. When the solution pH is adjusted to a pH of 5, a release of Hoechst into the solution was observed (Figure 4a). This result indicates that the IDA nanogate is tightly shut when latched with nickel and can also be used to deliver nickel ions after acidification. In an experiment similar to that of the cobalt-latched nanogate, the nickel-latched machine was also tested for release with competitive binding. A baseline fluorescence was also collected for a comparable time and released via the addition of bipy. Hoechst release is only observed after bipy addition, indicating a similar mechanism of trapping and release to that of the cobalt-latched nanogates (Figure S5, Supporting Information).

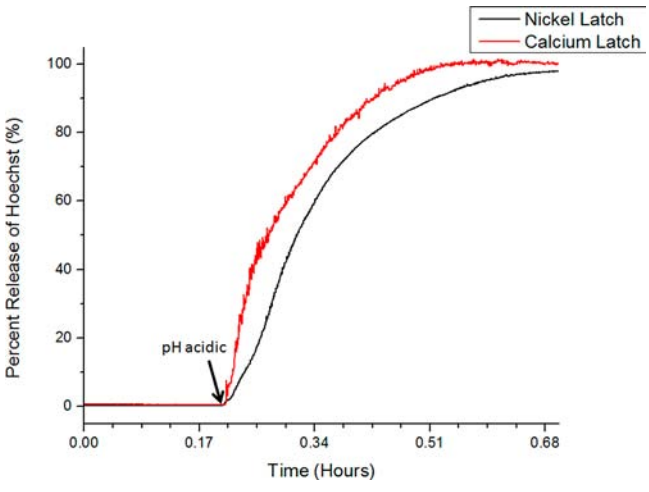

Figure 4. Time-resolved fluorescence spectra demonstrating the release of Hoechst cargo from nanogates assembled from nickel(II) (black trace) and calcium latches (red trace). No cargo release is observed from the nickel-latched nanogates until the solution pH is adjusted to pH 5. Cargo release is observed from the calcium-latched nanogates after adjusting the solution to a pH of 6, as a result of the lower binding constants between IDA and calcium. Release via competitive chelation is also demonstrated for the nickel-latched nanogate (Figure S5, Supporting Information).

Calcium Latch. Calcium, a metal ion with important biological significance, was also tested with this design. Because of its role as a regulator for cell apoptosis, a controlled delivery of calcium can potentially have therapeutic value. Therefore, the IDA nanogate system was tested for functionality with calcium ions. In a similar fashion as described above, Hoechst-loaded IDA nanoparticles were latched by introducing Ca^{2+}. A baseline was also collected for a comparable time to the previous experiments before stimulating cargo release through acidification. No Hoechst cargo was observed to release until the pH of the solution was adjusted to a pH of 6, indicating the compatibility of calcium ion as a latch for this system (Figure 4b). Because of the lower binding affinity between calcium and IDA, Hoechst release was observed to begin at a higher pH value than that for the nickel- and cobalt-latched nanomachines. Since the stability of the formed metal inorganic complex is metal-dependent, each nanogate built on a different metal center may be activated at different pHs, depending on the metal IDA binding strengths. Using this design, a metal center can be chosen that responds only to strongly acidic conditions or, if desired, a metal nanogate that responds to a more subtle pH change.

SUMMARY

In summary, a new type of nanogate supported on MSNs was successfully designed and synthesized. The fully assembled system is capable of simultaneously delivering both large and small molecules. In neutral conditions, the nanogate remains closed and cargo is stored, but the addition of acid opens the nanogate, releasing both metal ions and the large cargo molecules. Controlled cargo release was also demonstrated by activation through competitive binding. This system can potentially be expanded as a delivery system for a broad combination of cargo molecules and metal ions for biological application. By changing both the metal ion and/or the choice of nanogate, the pH responsiveness can be tuned to allow for biological pH activation. Currently, this system is being optimized using different transition-metal ions with the goal of developing a synergistic drug delivery system.

EXPERIMENTAL SECTION

General Comments. Chemicals used in this study were purchased from major chemical suppliers, such as Sigma-Aldrich and Fisher Scientific, and used without further purification. Release studies were obtained with an in-house time-resolved fluorescence spectroscopy setup (Figure S7, Supporting Information). A Coherent 377 nm CUBE laser was used to excite the Hoechst dye, and the subsequent emission spectra were monitored using a Princeton Instruments Roper CCD detector cooled to liquid nitrogen temperatures. ICP-OES measurements were made using a Thermo Jarrell Ash IRIS 1000 in a 5% HNO_3 matrix. XRD measurements were made using a Panalytical X'Pert Pro powder diffractometer. ^1H NMR was performed on a Bruker ARX400 spectrometer in $CDCl_3$ solution. Chemical shift is listed in parts per million. The solvent signal was used as an internal standard. Solid-state NMR was performed on a Bruker DSX300 spectrometer. TEM images were acquired on a JEM1200-EX microscope. SEM images were taken on a JSM-6701F microscope after coating with gold (5 nm) through plasma sputtering.

dx.doi.org/10.1021/ic3024265 | Inorg. Chem. 2013, 52, 2044−2049

Synthesis of MCM-41 Nanoparticles. In a 250 mL round-bottom flask equipped with a magnetic stir bar, cetyltrimethylammonium bromide (CTAB, 0.25 g, 0.7 mmol) was added and dissolved in deionized water (120 mL) with heat. The temperature was stabilized at 80 °C for 1 h, and a NaOH solution (2 M, 870 μL, 1.7 mmol) was added to the mixture at a rate to maintain 80 °C. Tetraethylorthosilicate (TEOS, 1.2 mL, 5.4 mmol) was then added dropwise over 10 min under vigorous stirring (800 rpm) and reacted for 2 h at 80 °C. After the allotted reaction time, the milky solution was allowed to cool to room temperature under stirring, and collected with centrifugation (7830 rpm, 15 min). The nanoparticles were washed with methanol until the washings showed a pH of 7. DLS readings of synthesized MSN in water indicate a low PDI (224 nm, PDI 0.01) on a ZetaPals instrument. MSN particle quality was confirmed through TEM/XRD measurements (Figures S1 and S2, Supporting Information).

Extraction of Templating Agent. In a 250 mL round-bottom flask, synthesized MSNs (120 mg) were suspended in methanol (75 mL) with vigorous stirring and water bath sonication. Under sonication, concentrated HCl (12 M, 4.2 mL) was added to the dropwise suspension where the solution became clearer, and refluxed for 8 h under an inert atmosphere. The particles were recollected through centrifugation (7830 rpm, 15 min) and washed with portions of methanol until washings showed a neutral pH. Complete extraction of CTAB from the pores was confirmed through IR spectroscopy (Figure S3, Supporting Information). Surfactant extracted particles gave a more monodisperse DLS reading in water (180 nm, PDI 0.005).

Synthesis of Dimethyl Iminodiacetate. In a 500 mL round-bottom flask equipped with a reflux condenser and a magnetic stir bar, iminodiacetic acid (5 g, 38 mmol) was suspended in methanol (200 mL). The solution was cooled to 0 °C while oxalyl chloride (7 mL, 82 mmol) was added to the reaction mixture in a dropwise fashion. After complete addition of the oxalyl chloride, the solution was warmed to room temperature and refluxed overnight. The solvent was evaporated off, giving a white powder (6 g). The powder was dissolved in water, neutralized with sodium carbonate, and extracted with ethyl acetate (3 × 35 mL). The combined organic layers were washed with brine (60 mL) and dried over anhydrous sodium sulfate, filtered, and concentrated under reduced atmosphere to give quantitative yields of a slightly yellow oil. ^{1}H NMR (chloroform-*d*): δ 2.01 (s, 1H), δ 3.36 (s, 4H), δ 3.61 (s, 6H).

Synthesis of (Dimethyl Iminodiacetate)-propyltriethoxysilane. In a 50 mL three-necked round-bottom flask equipped with a reflux condenser, gas inlet, and magnetic stir bar, dimethyl iminodiacetate (1 mL, 6 mmol) and 3-iodopropyltriethoxysilane (1 mL, 5 mmol) were dissolved in anhydrous toluene (5 mL). Catalytic amounts of *N*,*N*-diisopropylethylamine was added, and the mixture was allowed to react under a dry nitrogen atmosphere overnight at reflux. The mixture was then cooled to room temperature, washed with three portions of water and brine, and dried over anhydrous sodium sulfate. The organic layer was then concentrated under reduced pressure and purified with column chromatography oven-dried silica gel (CH_3Cl_3: hexanes = 2: 1) to yield quantitative amounts of (dimethyl iminodiacetate)propyltriethoxysilane. ^{1}H NMR (chloroform-*d*): δ 0.73 (t, 2H), δ 1.15 (t, 9H), δ 1.89 (m, 2H), δ 3.18 (t, 2H), δ 3.44 (s, 4H), δ 3.54 (q, 6H), δ 3.66 (s, 6H).

Synthesis of Dimethyl Iminodiacetate Modified Nanoparticles. In a 50 mL round-bottom flask, MSNs (50 mg) were washed with toluene (2 × 10 mL) and were suspended in anhydrous toluene dried over calcium hydride (10 mL). (Dimethyl iminodiacetate)propyltriethoxysilane (30 μL, 0.08 mmol) dissolved in toluene (1 mL) was added to the MSN suspension, which was heated overnight at reflux temperatures. The functionalized particles were collected through centrifugation (7830 rpm, 10 min) and washed with toluene (2 × 10 mL) and methanol (2 × 10 mL).

Synthesis of Iminodiacetic Acid Modified Nanoparticles (IDA-MSNs). A 50 mL round-bottom flask was charged with a suspension of dimethyl iminodiacetate modified silica nanoparticles (30 mg) in doubly distilled water (25 mL). Concentrated HCl (1.5 mL) was slowly added to the reaction mixture under sonication and refluxed for 6 h. The particles were recollected through centrifugation (7830 rpm, 10 min) and washed with methanol until the washings were of neutral pH. Successful functionalization of the silica surface was verified through solid-state NMR (Figures S4a and S4b, Supporting Information).

Loading of Hoechst 33342. IDA-MSN (10 mg) was washed twice with methanol and twice with doubly distilled water. After the solvent exchange, the particles were centrifuged and resuspended in a fresh solution of Hoechst 33342 in water (1 mM, 1 mL) and stirred overnight. The Hoechst-loaded particles were collected through centrifugation (15 000 rpm, 3 min) and dried under vacuum.

Closing of the Nanogate and Loading of the Smaller Cargo. Hoechst-loaded IDA-MSN (10 mg) was suspended in doubly distilled water (100 μL). For cobalt-closed nanogates, cobalt(II) chloride (20 mg, 0.15 mmol) was added to the mixture, and the mixture was stirred for 6 h. For nickel-closed nanogates, nickel(II) chloride (20 mg, 0.15 mmol) was added instead. For calcium-latched nanoparticles, calcium chloride (50 mg, 0.4 mmol) was added in a buffered solution (Tris buffered, pH 8), and the mixture was stirred overnight. The assembled machine was collected through centrifugation (15 000 rpm, 3 min), washed with doubly distilled water until the washings no longer exhibited fluorescence under black light, and dried under vacuum.

Assessment of the Cargo Release. Hoechst-loaded, metal-ion-capped IDA-MSNs (5 mg) were confined to a corner of a rectangular glass cuvette. To this, doubly distilled water (4 mL) was added to the particles at a rate to limit particles from suspending in solution. A 377 nm excitation diode laser (14 mW) was directed through the solution supernatant. The emission of excited Hoechst dye present in the solution supernatant was monitored in real time by focusing the emitted light through a collecting lens, a 400 nm cutoff filter, and a monochromator (300 nm window, centered on 500 nm) before integrating on a CCD detector (Figure S7, Supporting Information). A baseline was collected over 2 h of allowing suspended particles to settle before stimulating cargo release.

pH Activation. For pH-released samples, after achieving a stable baseline with the setup as described above, a known quantity of dilute HCl freshly calibrated was added to adjust the solution pH to 5. A plot of fluorescence intensity with respect to time was generated through integrating fluorescence counts from 500 to 550 nm. After complete release, the supernatant was collected through centrifugation (7830 rpm, 25 min) and analyzed through UV−vis to determine weight percent release of Hoechst dye. The amount of cobalt released was done through stabilizing dissolved metals by adding 70% HNO_3 (307 μL) to the release supernatant and analysis with ICP-OES. Intensity of the analyzed samples was standardized using standard solutions made by diluting a stock solution (1000 ppm, Fisher Scientific) of cobalt or nickel or calcium. Each sample was run 3× to generate statistical data and error.

Competitive Binding Activation. For the nickel-latched nanogate, after achieving a stable baseline plot with the above setup, solid 2,2′-bipyridine (15 mg) was added to the solution to saturate the solution. Competitive binding release studies with the cobalt-latched nanogate were performed by adding 100 μL of a saturated solution of bipy in water to the 4 mL sample.

■ ASSOCIATED CONTENT

Ⓢ Supporting Information

Experimental, materials and methods, XRD of synthesized MSN, solid-state ^{13}C and ^{29}Si NMR data, time-resolved fluorescent spectra release profiles of Ni^{2+} and Ca^{2+} latches with acid and competitive binding activation, and UV−vis spectra of cobalt IDA complexes after simulated loading conditions. This material is available free of charge via the Internet at http://pubs.acs.org.

AUTHOR INFORMATION

Corresponding Author

*E-mail: zink@chem.ucla.edu.

Notes

The authors declare no competing financial interest.

ACKNOWLEDGMENTS

This work was supported by grant NIH RO1 CA133697. The authors also acknowledge David Weiler for helpful discussions.

REFERENCES

(1) Browne, R. W.; Feringa, L. B. *Nat. Nanotechnol.* **2006**, *1*, 25−35.
(2) Lin, Y.-S.; Hurley, K. R.; Haynes, C. L. *J. Phys. Chem. Lett.* **2012**, *3*, 364−374.
(3) Cheon, J.; Lee, J. H. *Acc. Chem. Res.* **2008**, *41*, 1630−1640.
(4) Ambrogio, W. M.; Thomas, R. C.; Zhao, Y.; Zink, I. J.; Stoddart, J. F. *Acc. Chem. Res.* **2011**, *44*, 903−913.
(5) Slowing, I. I.; Trewyn, G. B.; Giri, S.; Lin, S. V. *Adv. Funct. Mater.* **2007**, *17*, 1225−1236.
(6) Davis, M. E. *Nature* **2002**, *417*, 813−821.
(7) Zhao, S. X.; Lu, Q. G.; Whittaker, K. A.; Millar, J. G.; Zhu, Y. H. *J. Phys. Chem. B* **1997**, *101*, 6525−6531.
(8) Vallet-Regi, M.; Ramila, A.; del Real, P. R.; Perez-Pariente, J. *Chem. Mater.* **2001**, *13*, 308−311.
(9) Kruk, M.; Jaroniec, M. *J. Phys. Chem. B* **1997**, *101*, 583−589.
(10) Slowing, I. I.; Escoto-Vivero, J. L.; Wu, C.-W.; Lin, V. S.-Y. *Adv. Drug Delivery Rev.* **2008**, 1278−1288.
(11) Nguyen, T. D.; Tseng, H. R.; Celestre, P. C.; Flood, A. H.; Liu, Y.; Stoddart, J. F.; Zink, J. I. *Proc. Natl. Acad. Sci. U.S.A.* **2005**, *102*, 10029−10034.
(12) Trewyn, B. G.; Slowing, I. I.; Giri, S.; Chen, H.-T.; Lin, V. S.-Y. *Acc. Chem. Res.* **2007**, *40*, 846−853.
(13) Ferris, D. P.; Zhao, Y.-L.; Khashab, N. M.; Khatib, H. A.; Stoddard, J. F.; Zink, J. I. *J. Am. Chem. Soc.* **2009**, *131*, 1686−1688.
(14) Zhao, Y.; Li, Z.; Kabehie, S.; Botros, Y. Y.; Stoddart, J. F.; Zink, J. I. *J. Am. Chem. Soc.* **2010**, *132*, 13016−13025.
(15) Meng, H.; Xue, M.; Xia, T.; Zhao, Y.; Tamanoi, F.; Stoddart, J. F.; Zink, J. I. *J. Am. Chem. Soc.* **2010**, *132*, 12690−12697.
(16) Coti, K. K.; Belowich, M. E.; Liong, M.; Ambrogio, M. W.; Lau, T. A.; Khatib, H. A.; Zink, J. I.; Khashab, N. M.; Stoddart, J. F. *Nanoscale* **2009**, *1*, 16−39.
(17) Li, Z.; Barnes, J. C.; Bosoy, A.; Stoddart, J. F.; Zink, J. I. *Chem. Soc. Rev.* **2012**, *41*, 2590−2605.
(18) Patel, K.; Angelos, S.; Dichtel, W. R.; Coskun, A.; Yang, Y.-W.; Zink, J. I.; Stoddart, J. F. *J. Am. Chem. Soc.* **2008**, *130*, 2382−2383.
(19) Fu, Q.; Rao, V.-R.; Ista, L. K.; Wu, Y.; Andrzejewski, B. P.; Sklar, L. A.; Ward, T. L.; Lopez, G. P. *Adv. Mater.* **2003**, *15*, 1262−1266.
(20) Vivero-Escoto, J. L.; Slowing, I. I.; Trewyn, B. G.; Lin, V. S.-Y. *Small* **2010**, *6*, 1952−1967.
(21) Climent, E.; Martínez-Máñez, R.; Sancenón, F.; Marcos, M. D.; Soto, J.; Maquieira, A.; Amorós, P. *Angew. Chem., Int. Ed.* **2010**, *49*, 7281−7283.
(22) Mal, N. K.; Fujiwari, M.; Tanaka, Y. *Nature* **2003**, *23*, 350−353.
(23) Thomas, C. R.; Ferris, D. P.; Lee, J. H.; Choi, E.; Kim, E. S.; Stoddart, J. F.; Shin, J. S.; Cheon, J.; Zink, J. I. *J. Am. Chem. Soc.* **2010**, *132*, 10623−10625.
(24) Lu, J.; Choi, E.; Tamanoi, F.; Zink, J. I. *Small* **2008**, *4*, 421−426.
(25) Mal, N. K.; Fujiwara, M.; Tanaka, Y.; Taguchi, T.; Matsukata, M. *Chem. Mater.* **2003**, *15*, 3385−3394.
(26) Lu, J.; Liong, M.; Zink, J. I.; Tamanoi, F. *Small* **2007**, *3*, 1341−1346.
(27) Zheng, H.; Huang, Z.; Che, S. *Dalton Trans.* **2012**, *41*, 5038.
(28) Chouyyok, W.; Shin, Y.; Davidson, J.; Samuels, W.; La Fermina, H. N.; Rutledge, D. R.; Fryxell, G.; Sanvanich, T.; Yantasee, W. *Environ. Sci. Technol.* **2010**, *44*, 6390−6395.
(29) Busche, B.; Wiacek, R.; Davidson, J.; Koonsiripaiboon, V.; Yantasee, W.; Addelman, R. S.; Fryxell, E. G. *Inorg. Chem. Commun.* **2009**, *12*, 312−315.
(30) Young, R. S. *Cobalt in Biology and Biochemistry*; Academic Press Inc: London, 1979.
(31) Denkhaus, E.; Salnikow, K. *Crit. Rev. Oncol. Hematol.* **2002**, *42*, 35−56.
(32) Mattson, M. P.; Chan, S. L. *Nat. Cell Biol.* **2003**, *5*, 1041−1043.
(33) Orrenius, S.; Zhivotovsky, B.; Nicotera, P. *Nat. Rev. Mol. Cell Biol.* **2003**, *4*, 552−565.
(34) Hofer, A. M.; Brown, E. M. *Nat. Rev. Mol. Cell Biol.* **2003**, *4*, 530−538.
(35) Rizzuto, R.; Pinton, P.; Ferrari, D.; Chami, M.; Szabadkai, G.; Magalhães, P. J.; Virgilio, F. D.; Pozzan, T. *Oncogene* **2003**, *22*, 8619−8627.
(36) Bernauer, L.; Walz, D.; Fallab, S. *Helv. Chim. Acta* **1958**, *41*, 2094−2099.
(37) Schwarzenbach, G.; Anderegg, G.; Schneider, W.; Senn, H. *Helv. Chim. Acta* **1955**, *38*, 1147.
(38) Irving, H.; Mellor, D. H. *J. Chem. Soc.* **1962**, 5222−5237.
(39) Angelos, S.; Liong, M.; Choi, E.; Zink, J. I. *Chem. Eng. J.* **2008**, *137*, 4−13.
(40) Hiemstra, T.; de Wit, J. C. M.; van Riemsdijk, W. H. *J. Colloid Interface Sci.* **1989**, *133*, 105−117.
(41) Li, Z.; Nyalosaso, L. J.; Hwang, A. A; Ferris, P. D.; Yang, S.; Derrien, G.; Charnay, C.; Durand, J. O.; Zink, J. I. *J. Phys. Chem. C* **2011**, *115*, 19496−19506.